Understanding Copper Trafficking in Bacteria: Interaction between the Copper Transport Protein CopZ and the N-Terminal Domain of the Copper ATPase CopA from *Bacillus subtilis*[†]

Lucia Banci, Ivano Bertini,* Simone Ciofi-Baffoni, Rebecca Del Conte, and Leonardo Gonnelli

Department of Chemistry and Centro Risonanze Magnetiche, University of Florence, Via Luigi Sacconi 6, 50019 Sesto Fiorentino (Florence), Italy

ABSTRACT: In this paper the interaction of cytoplasmic CopZ and the N-terminal domain of the CopA ATPase from *Bacillus subtilis* has been studied by NMR through ^{15}N−^{1}H HSQC experiments in order to understand the role of the two proteins in the whole copper trafficking mechanism of the bacteria. It appears that the two proteins interact in a fashion similar to that of the yeast homologue proteins [Arnesano, F., Banci, L., Bertini, I., Cantini, F., Ciofi-Baffoni, S., Huffman, D. L., and O'Halloran, T. V. (2001) *J. Biol. Chem. 276*, 41365−41376], although the surface potentials are reversed. A structural model for the interaction is proposed. ^{15}N mobility studies on the free proteins and on their complex are also reported. From these data, it appears that copper is largely transferred from CopZ to CopA, thus suggesting their possible involvement in a detoxification process. Comparing functional data of homologous proteins of other bacteria, it can be concluded that this class of proteins is involved in copper homeostasis but the specific roles are species dependent.

The intracellular concentration of copper is controlled by a number of proteins in order to avoid excess of this toxic, redox-active ion and at the same time to provide sufficient amounts of it for copper-dependent enzymes (*1−3*). Therefore, import, export, and sequestration mechanisms are required to balance and guarantee the safety of cells. Yeast cells have provided an excellent model system for studies of copper transport, distribution, and detoxification. Copper uptake in *Saccharomyces cerevisiae* is mediated by the CTR plasma membrane proteins (*4−7*). Once inside the cell, a pathway for copper delivery to multicopper oxidases involves the chaperone Atx1 and a CPx-type ATPase, Ccc2, which pumps this metal ion through the post-Golgi membrane (*8−10*). Recently, the interaction between Atx1 and Ccc2a, whose solution structures are available (*11, 12*), was analyzed, and a mapping of surface residues involved in protein−protein recognition was provided (*13*). In bacteria, copper uptake into the cell and its transport to the specific proteins are much less characterized (*14, 15*). The best studied copper transport system involves copper ATPase proteins CopA, CopB and the copper chaperone CopZ from *Enterococcus hirae* (*16−18*). It was reported that CopA is responsible for copper uptake under copper limiting conditions, that CopB is responsible for copper export, and that the chaperone CopZ specifically binds to CopA and to its repressor CopY (*16, 19, 20*). Two copper proteins, with sequence identity >30% and homologues of CopZ and CopA

from *E. hirae*, are present in the genome of *Bacillus subtilis* bacteria (*21*). The protein with 45% sequence identity to *E. hirae* CopA, hereafter BsCopA, is a membrane protein which has two N-terminal domains each containing a MXCXXC motif, a metal-binding domain typical of Cu binding CPx-type ATPases (*22*). Also, the protein from *B. subtilis* with 39% sequence identity to CopZ from *E. hirae* (BsCopZ, hereafter) contains the classical copper binding MXCXXC motif. BsCopZ and the second N-terminal domain of BsCopA (BsCopAb, hereafter) were expressed, and their solution structures were determined with and without copper (*22, 23*). The second N-terminal domain was chosen instead of the first N-terminal domain since the latter is in an unfolded state (*22*). All of these structures share a classical "ferredoxin-like" $\beta 1-\alpha 1-\beta 2-\beta 3-\alpha 2-\beta 4$ folding (*24*). The two cysteines of the MXCXXC motif are located both in BsCopZ and in BsCopAb, one in the first loop and the other at the beginning of the first α-helix. BsCopAb has a positively charged region on its surface, while BsCopZ has multiple negatively charged regions. Transfer between two possible protein partners has been suggested on the basis of complementary electrostatic forces that ultimately orient the metal-binding loops of the chaperone and of the ATPase domains for formation of copper-bridged ligand intermediates (*25*). However, it is important to ascertain whether copper is physiologically transferred from CopA to CopZ or vice versa in *B. subtilis* and to figure out whether the copper trafficking in bacteria varies from one species to another.

With this aim, the interaction of the BsCopZ copper transport protein with BsCopAb was investigated through ^{1}H and ^{15}N chemical shift perturbation experiments by titrating Cu(I)-BsCopZ with apo-BsCopAb and vice versa.

* To whom correspondence should be addressed. Fax: +39.055.4574271. Phone: +39.055.4574270. E-mail: bertini@cerm.unifi.it.

Table 1: Acquisition Parameters for NMR Experiments

experiments	dimension of acquired data (nucleus)			spectral width (ppm)			n^a	ref
	t_1	t_2	t_3	F_1	F_2	F_3		
^{1}H$-$^{15}N HSQC	256 (^{15}N)	1024 (^{1}H)		40	16		4	57
[^{1}H$-$^{1}H] NOESY	2048 (^{1}H)	1024 (^{1}H)		16	16		64	58
^{15}N-edited [^{1}H$-$^{1}H] NOESY	256 (^{1}H)	40 (^{15}N)	1024 (^{1}H)	16	40	16	24	59
[^{1}H$-$^{1}H] TOCSY	2048 (^{1}H)	1024 (^{1}H)		16	16		32	60

^{a} Number of acquired scans.

The results suggest that the two proteins interact, that a single copper ion is largely associated with BsCopA rather than with BsCopZ, and that the exchange between free proteins and the complex is relatively fast. A mapping of surface residues involved in protein–protein recognition and interaction is provided together with a structural model of the two proteins in the complex. Dynamical characterization of the system suggests an equilibrium between the homodimeric CopZ and a heterodimeric species composed of one CopZ monomer and one CopAb monomer. This complex likely allows for the transfer of copper under physiological conditions. A genomic analysis allows us to discuss comparatively possible differences in trafficking mechanisms in several bacterial organisms.

EXPERIMENTAL PROCEDURES

Sample Preparation. BsCopZ and BsCopAb (construct 73–151 of the CopA ATPase) and their copper derivatives were obtained in the *Escherichia coli* BL21(DE3)*plysS* strain (Novagene) following previously published protocols (*22, 23*). For BsCopAb residues 72–151 have been renumbered as 1–80 for easy comparison with BsCopZ. The labeling was performed by growing the cells in the labeled Silantes medium, *E. coli* OD2-N, at variance with the previous preparations (*22, 23*). All manipulations, after the purification, were performed in an inert nitrogen atmosphere.

The NMR samples had an initial concentration of about 1–2 mM protein with 1 equiv of DTT[1] in 100 mM phosphate buffer at pH 7.0 and 10% D$_2$O for the lock signal.

NMR Titration of the Two Proteins. Titrations of one protein, with increasing amounts of the other, were followed through ^{15}N$-$^{1}H HSQC spectra to detect changes in the spectral features. Aliquots were added in a Coy chamber under a nitrogen atmosphere at 298 K using a Hamilton syringe. To samples of labeled proteins with an initial concentration around 1–2 mM, additions ranging from 0.045 to 1.05 mM in the partner protein were performed to reach about a 1:1 protein ratio.

NMR Spectroscopy. All of the NMR spectra were acquired at 298 K on a 600 or a 700 Bruker spectrometer operating at proton nominal frequencies of 600.13 and 700.13 MHz, respectively. A triple resonance (TXI) 5 mm probe, equipped with pulsed field gradients (PFG) along the *z*-axis, was used.

The NMR experiments, performed to detect the spectral changes during the titrations and to have the assignment of ^{15}N$-$^{1}H HSQC spectra, are summarized in Table 1. 2D and 3D NOESY and TOCSY experiments on the complexes were recorded with a protein concentration ratio of 1:0.5 and 1:1.

All of the relaxation experiments, except those on Cu(I)-BsCopAb performed at 700 MHz, were carried out at 600 MHz. The backbone ^{15}N longitudinal R_1 and transverse R_2 relaxation rates were measured as previously described (*26*) using delays (*T*) in the pulse sequence, from 10 to 2500 ms for R_1 and from 7.8 to 357.0 ms with a refocusing delay (τ_{CPMG}) of 450 μs for R_2, for all of the samples. The recycle delay was set to 2.5 s for all measurements. Transverse relaxation rates were also measured as a function of τ_{CPMG} with values ranging from 450 to 1150 μs to monitor conformational exchange processes (*27, 28*). In these measurements relaxation delay varied from 7 to 230 ms, the exact values depending on τ_{CPMG}. For all of these experiments, the 2D spectra, acquired with 8 or 16 scans, consisted of 1024 data points in the acquisition dimension and of 256 experiments in the indirect dimension.

Quadrature detection in the indirect dimensions was performed in the TPPI mode (*29*). Water suppression was achieved through the WATERGATE sequence (*30*), except for R_1 and R_2 experiments where flip-back pulses were used (*31*). All of the spectra were processed using the standard Bruker software (XWINNMR) and analyzed through the XEASY program (*32*). Integration of cross-peaks in the R_1 and R_2 measurements was performed by using the standard routine of the XWINNMR program.

Relaxation Data Analysis. Relaxation rates R_1 and R_2 were determined by fitting the cross-peak intensities (*I*) measured as a function of the delay (*T*) within the pulse sequence, to a single-exponential decay. Errors on the rates were estimated through a Monte Carlo approach (*33–35*). The overall tumbling correlation time and the local correlation times for the NH vector of each residue were estimated from the measured R_2/R_1 ratios using the model-free approach (*36*). In this analysis the relaxation rates of NHs experiencing exchange processes, which can contribute to R_2 values with a R_{ex} contribution, were discarded. Residues are considered as experiencing conformational exchange processes if the following condition applies (*37*):

$$(\langle 1/R_2 \rangle - 1/R_{2n})/\langle 1/R_2 \rangle - (\langle 1/R_1 \rangle - 1/R_{1n})/\langle 1/R_1 \rangle >$$
$$1.5\text{SD} \quad (1)$$

where R_{2n}, R_{1n} are the R_2, R_1 values of residue n and $\langle 1/R_2 \rangle$, $\langle 1/R_1 \rangle$ are the average rates. SD is the standard deviation of $(\langle 1/R_2 \rangle - 1/R_{2n})/\langle 1/R_2 \rangle - (\langle 1/R_1 \rangle - 1/R_{1n})/\langle 1/R_1 \rangle$.

The presence of exchange processes occurring with correlation times, τ_{ex}, in the range between 500 and 100 μs

---

[1] Abbreviations: DTT, dithiothreitol; NOE, nuclear Overhauser effect; HSQC, heteronuclear single-quantum coherence; NOESY, nuclear Overhauser effect spectroscopy; TOCSY, total correlation spectroscopy; R_1, longitudinal relaxation rate; R_2, transverse relaxation rate; CPMG, Carr–Purcell–Meiboom–Gill; TPPI, time-proportional phase incrementation; WATERGATE, water suppression by gradient-tailored excitation; Tris, tris(hydroxymethyl)aminomethane; MES, 2-(*N*-morpholino)ethanesulfonic acid.

was determined through R_2 measurements as a function of τ_{CPMG} delay.

The exchange contribution R_{ex} to R_2 can be expressed in terms of the weak effective magnetic field, ν_{eff}, which is produced by the CPMG pulse train in the *xy* plane by the equation (*38*):

$$R_{2,ex} = \frac{k_{ex}}{2} - 2\nu_{eff} \sinh^{-1}\left(\frac{k_{ex}}{\xi} \sinh \frac{\xi}{4\nu_{eff}}\right) \qquad (2)$$

where $\xi = (k_{ex}^2 - 4p_A p_B \delta\omega^2)^{1/2}$ and $k_{ex} = 1/\tau_{ex}$. The effective magnetic field is related to the τ_{CPMG} length by the equation:

$$\nu_{eff}(s^{-1}) = \frac{1}{2(T_\pi + \tau_{CPMG})} \qquad (3)$$

where T_π is the duration of a 180° ^{15}N CPMG pulse (70 μs for the experiments collected at 600 MHz).

RESULTS

Titrations of Cu(I)-BsCopZ with Apo-BsCopAb. The ^{15}N$-^1$H HSQC spectra were measured for the copper-loaded and apo forms of both BsCopZ and BsCopAb for references purposes.

The ^{15}N$-^1$H HSQC map of Cu(I)-^{15}N BsCopZ showed the presence of only one form, i.e., the major form (named A) previously characterized (*23*). The minor form B, observed in previous preparations (*23*), is not present when the labeled sample is prepared as described in Experimental Procedures. All of the expected cross-peaks for the amide protons are present, even if the peaks of residues 13 and 14 are broader than the others. The metal-binding residues are Cys 13 in loop 1 and Cys 16 at the N-terminus of helix α1. The apo form displays two conformations, in a 70:30 ratio, for some residues belonging to loop 5 (62, 64−67) and helix α1 (22−25), as previously reported (*23*). Cross-peaks are missing in the apo form for residues 13−15 (loop 1), whereas cross-peaks of residues 11, 12, and 16−21 (loop 1 and helix α1) are significantly broadened. The different behavior of apo-BsCopZ with respect to the copper-loaded form reflects a larger flexibility in the copper binding region when the metal is absent.

In the ^{15}N$-^1$H HSQC spectrum of apo-^{15}N BsCopAb, NH cross-peaks for residues 2 (here, for comparison purposes with BsCopZ, residues 72−151 are renumbered as 1−80), 15, and 16 (loop 1) were not present, while in the copper-bound form only NH cross-peaks of residues 2 and 15 are not detected. Also in the apo form of BsCopAb two conformations were observed for a few residues belonging to loop 1 and helix α1 (12, 18−21, and 23−24) with a ratio of 90:10. These features are consistent with literature data (*22*).

The interaction between Cu(I)-BsCopZ and apo-BsCopAb was followed through two different titrations: (1) Cu(I)-^{15}N BsCopZ was titrated with unlabeled apo-BsCopAb; (2) apo-^{15}N BsCopAb was titrated with Cu(I)-^{15}N BsCopZ. The comparison between the two titrations allowed us to discriminate those resonances of the two proteins which are overlapped in the spectra of the latter titration. As expected, the ^{15}N$-^1$H HSQC spectra of the final 1:1 mixtures of the two titrations are the same, indicating that the same species

are present in solution starting either from Cu(I)-BsCopZ or from apo-BsCopA.

Several ^{1}H and ^{15}N resonances of Cu(I)-BsCopZ showed changes in chemical shift values upon addition of increasing amounts of apo-BsCopAb (Figure 1). In the 1:1 mixture, the cross-peaks of Ser 12, Cys 13, Gln 14, His 15, and Cys 16 of BsCopZ broadened beyond detection. Twenty-two backbone NHs (8−11, 17−25, 37, 59, 62−68) and the N$_\epsilon$H$_2$ of Gln 14 and Gln 63 had measurable changes in chemical shift values throughout the titration. Of the latter backbone NHs, 18 (8−11, 20−25, 59, 62−68) also experience splitting of the signals as the titrant concentration increases (Figure 1), indicating the presence of two conformations in slow exchange with one another. All of these residues are located around the metal-binding region and behave in a fashion similar to that of apo-BsCopZ, in particular in terms of splitting. The analysis of the ^{1}H, ^{15}N, and weighted-average (*39*) chemical shift value differences between Cu(I)-^{15}N BsCopZ alone and in the 1:1 mixture (Figure 2)[2] highlights that the largest spectral changes in Cu(I)-^{15}N BsCopZ upon addition of apo-BsCopAb are located in loop 1, helix α1, the last turn of helix α2, and loop 5.

Concerning BsCopAb, ^{15}N$-^1$H HSQC cross-peaks of residues around the copper binding region (11, 12, 18−20, 22−24, 26, 61, 63−64, 67−68) showed measurable changes in chemical shift values (Figure 3) upon increased concentrations of Cu(I)-BsCopZ. The cross-peaks of residues 13, 14, 17, and 21 (loop 1 and helix α1) broadened and eventually disappeared during the titration. This suggests that the exchange regime between the complex and the free proteins is not fast enough with respect to the chemical shift changes. Indeed, these residues experience the largest chemical shift variations between the apo and the copper-loaded forms. Moreover, residues 12, 18, and 19, adjacent to the metal-binding ligands and still detected in the 1:1 complex, have chemical shift values very close to those of the Cu(I)-BsCopAb form, indicating that the chemical shift variations of these residues in the complex are similar to those obtained on going from apo- to Cu(I)-BsCopAb. The ^{1}H, ^{15}N, and weighted-average chemical shift differences between apo-^{15}N BsCopAb alone and in the 1:1 mixture show that the major changes in the apo form signals, when interacting with Cu(I)-BsCopZ, are located in two regions of the protein, stretch 12−26, which contains loop 1 and the first turn of helix α1, and stretch 61−68, which contains the last segment of helix α2 and the last loop (loop 5). On the other hand, chemical shift differences between Cu(I)- and apo-^{15}N BsCopAb were found mainly in the region 13−21 (loop 1 and helix α1) (Figure 3, right panel).

Analysis of 3D NOESY−^{15}N HSQC and 2D NOESY and TOCSY maps of the final mixtures for both titrations was used to confirm the assignment of the ^{15}N$-^1$H HSQC spectra of the major form of BsCopZ and to extend it to the minor one, and of BsCopAb. The TOCSY map was used to identify the spin patterns of the various amino acids. Then, these residues were connected to other spin patterns by characteristic sequential NOESY peaks. The 3D NOESY map was used to solve cross-peak overlap in the 2D NOESY map and to confirm the assignment of the ^{15}N resonances.

---

[2] $\{[(\Delta H)^2 + (\Delta N/5)^2]/2\}^{1/2}$, where ΔH and ΔN are chemical shift differences for ^{1}H and ^{15}N, respectively.
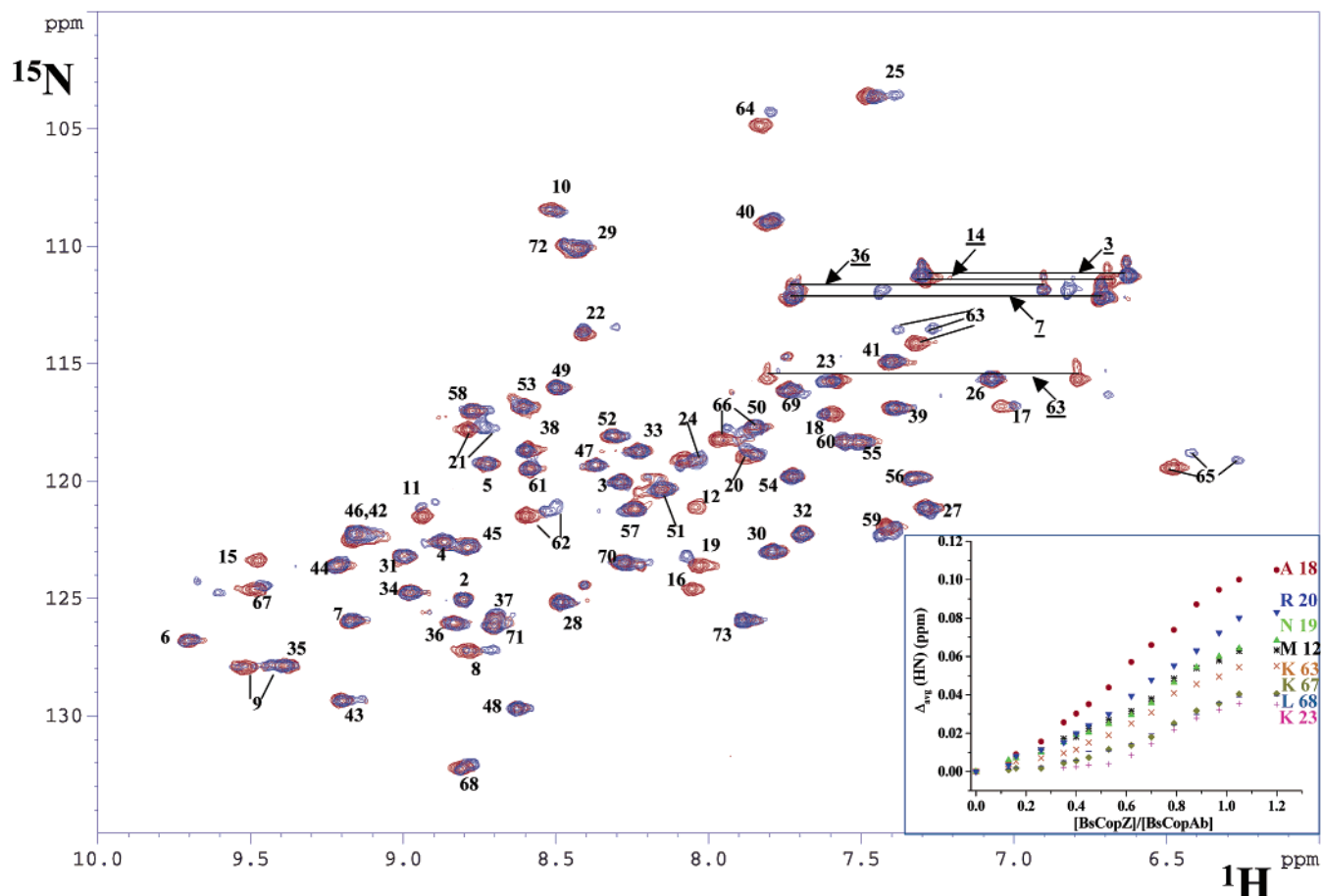
FIGURE 1: $^{15}N-^{1}H$ HSQC spectra (600 MHz, 298 K) of Cu(I)-^{15}N BsCopZ (red) and of the ^{15}N BsCopZ:BsCopAb (1:1) mixture (blue) (titration 1; see text). The peaks due to side chain NHs are indicated with underlined numbers. The inset shows the weighted-average chemical shift differences $\Delta_{avg}(HN)$ (see text) for some BsCopAb residues around the metal site as a function of BsCopZ concentration as measured in titration 2, performed using ^{15}N BsCopAb (see text).

Titration of Cu(I)-BsCopAb with Apo-BsCopZ. When Cu-(I)-^{15}N BsCopAb is titrated with increasing amounts of unlabeled apo-BsCopZ, residues of BsCopA showing chemical shift changes are essentially the same as found in the previous titration where the copper ion is initially bound to BsCopZ. The same happened for the cross-peaks that broadened and eventually disappeared. Moreover, if we compare the $^{15}N-^{1}H$ HSQC spectra of the final 1:1 mixtures of the two titrations [Cu(I)-^{15}N BsCopAb:apo-BsCopZ with apo-^{15}N BsCopAb:Cu(I)-^{15}N BsCopZ], we can observe that the $^{15}N-^{1}H$ HSQC spectrum of BsCopA is the same, indicating that the same species are obtained in solution starting the titrations either from Cu(I)-BsCopAb or from apo-BsCopAb. In Figure 4 the $^{15}N-^{1}H$ HSQC spectrum of Cu(I)-^{15}N BsCopAb (red contours) is compared with that of the Cu(I)-^{15}N BsCopAb:apo-BsCopZ (1:1) mixture (blue contours). The two species have similar spectra indicating that, in the complex, copper is mainly bound to BsCopAb. Resonances of residues 12, 18, and 19 belonging to the copper binding region of BsCopAb show minor chemical shift changes in the present titrations with respect to those observed in the previous titrations, confirming that BsCopAb in the complex is largely in the copper-bound form. The chemical shift variations for some residues of Cu(I)-^{15}N BsCopAb are also reported in the inset. From the comparison with the inset of Figure 1 it is evident that, when starting from apo-BsCopAb, the chemical shift changes observed for

residues 12, 18, and 19 are larger than in the present titration (inset of Figure 4). The midpoint of the spectral changes in both titrations occurred when the BsCopAb:BsCopZ ratio is about 1:0.65 (insets of Figure 1 and of Figure 4). This indicates that the two association processes occur with a similar dissociation constant. By fitting the titration data to a simple three-component model in which BsCopZ interacts with BsCopA to form a complex (intermediate), we can estimate a K_d in the range of $\sim 10^{-4}-10^{-5}$ M for both titrations, which is comparable with that found for the Atx1/Ccc2a complex (*13*).

Dynamic Characterization of BsCopAb and BsCopZ. The dynamic properties of both the apo and Cu(I) forms of ^{15}N BsCopAb and of Cu(I)-BsCopZ are also relevant for a complete characterization of the interaction between BsCopZ and BsCopAb (Figure 5). R_2 and R_1 were measured for those ^{15}N resonances that do not show overlap and therefore can be accurately integrated and analyzed as described in Experimental Procedures. For Cu(I)- and apo-BsCopAb, 69 and 68 ^{15}N nuclei were respectively analyzed. The average values of R_2 and R_1 rates are 7.34 ± 0.70 s^{-1} and 1.69 ± 0.07 s^{-1} for the copper-bound form and 7.89 ± 0.59 s^{-1} and 1.89 ± 0.12 s^{-1} for the apo form, respectively. For both forms of BsCopA, residues characterized by R_2 values lower more than 1σ from the mean value are located in the C-terminal part of the protein (residues 72–80). Indeed, the C-terminal region of BsCopA is disordered consistently also
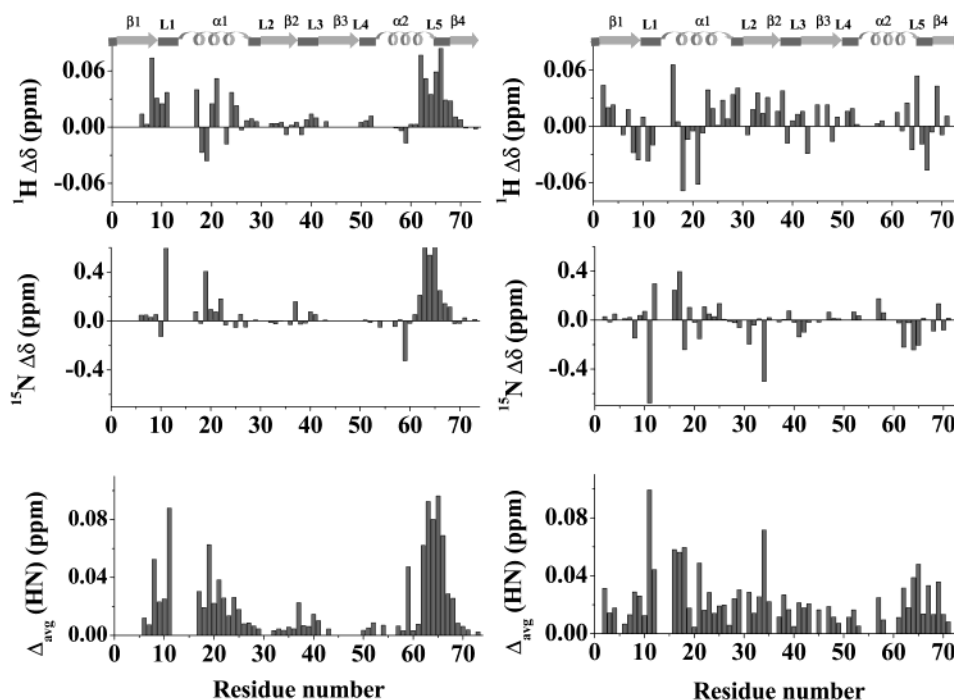
FIGURE 2: ^{1}H and ^{15}N amide chemical shift differences between the isolated Cu(I)-^{15}N BsCopZ and the ^{15}N BsCopZ:BsCopAb (1:1) mixture (left side) or the apo-^{15}N BsCopZ (right side). The weighted-average chemical shift differences Δ_{avg}(HN) (see text) are shown in the bottom plots. Chemical shift differences are not reported for residues 12−16 on the left side plots and for residues 13−15 on the right side plots, as these residues are not observed in one of the pairs of the comparison. The secondary structure elements of Cu(I)-BsCopZ are reported at the top.
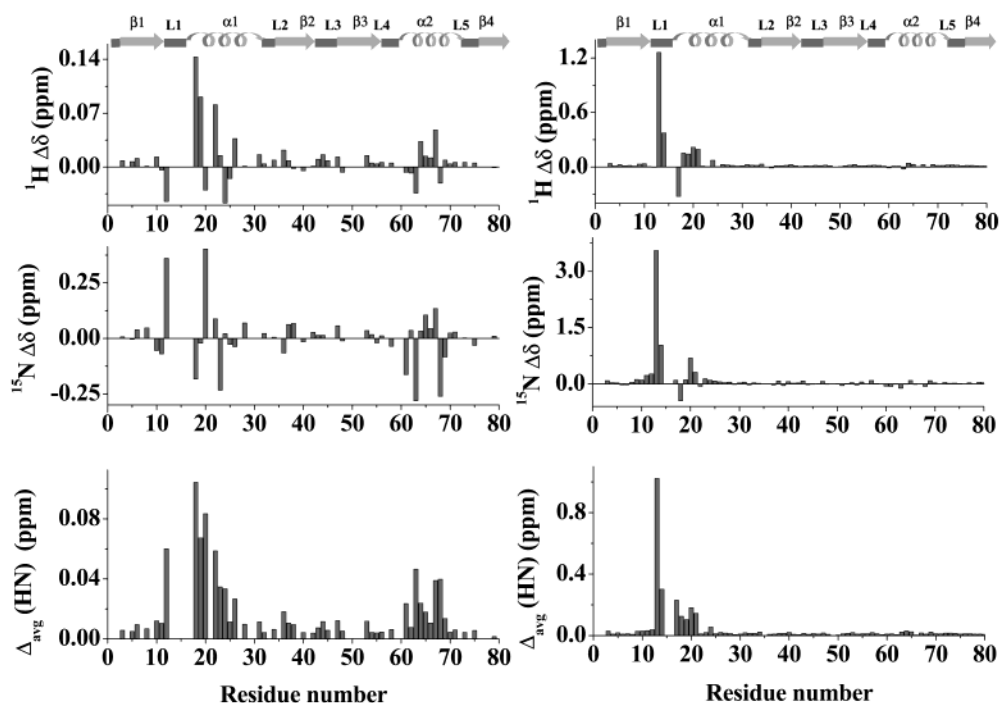

FIGURE 3: ^{1}H and ^{15}N amide chemical shift differences between the pure apo-^{15}N BsCopAb and the BsCopZ:BsCopAb (1:1) mixture (left side) or the Cu(I)-^{15}N BsCopAb (right side). The weighted-average chemical shift differences Δ_{avg}(HN) (see text) are shown in the bottom plots. Chemical shift differences are not reported for residues 13−17 and 21 on the left side plots and for residues 15 and 16 on the right side plots, as these residues are not observed in one of the pairs of the comparison. The secondary structure elements of apo-BsCopAb are reported at the top.

with the lack of medium- and long-range NOEs (22). The R_2 and R_1 values of the apo and copper-loaded proteins are quite homogeneous and show a very similar trend. From the R_2/R_1 ratios, τ_m values of 5.6 $\pm$ 0.4 and 5.0 $\pm$ 0.4 ns were estimated for apo- and Cu(I)-^{15}N BsCopAb, respectively. These values are consistent with those estimated from a

Stokes−Einstein isotropic model for a protein of this size in a monomeric state.

The R_2 and R_1 rates of the backbone amide nitrogens of Cu(I)-^{15}N BsCopZ were measured for 70 ^{15}N nuclei, which give average values of 12.51 $\pm$ 1.60 s^{-1} and 1.29 $\pm$ 0.09 s^{-1}, respectively (Figure 5). The τ_m value of the copper-
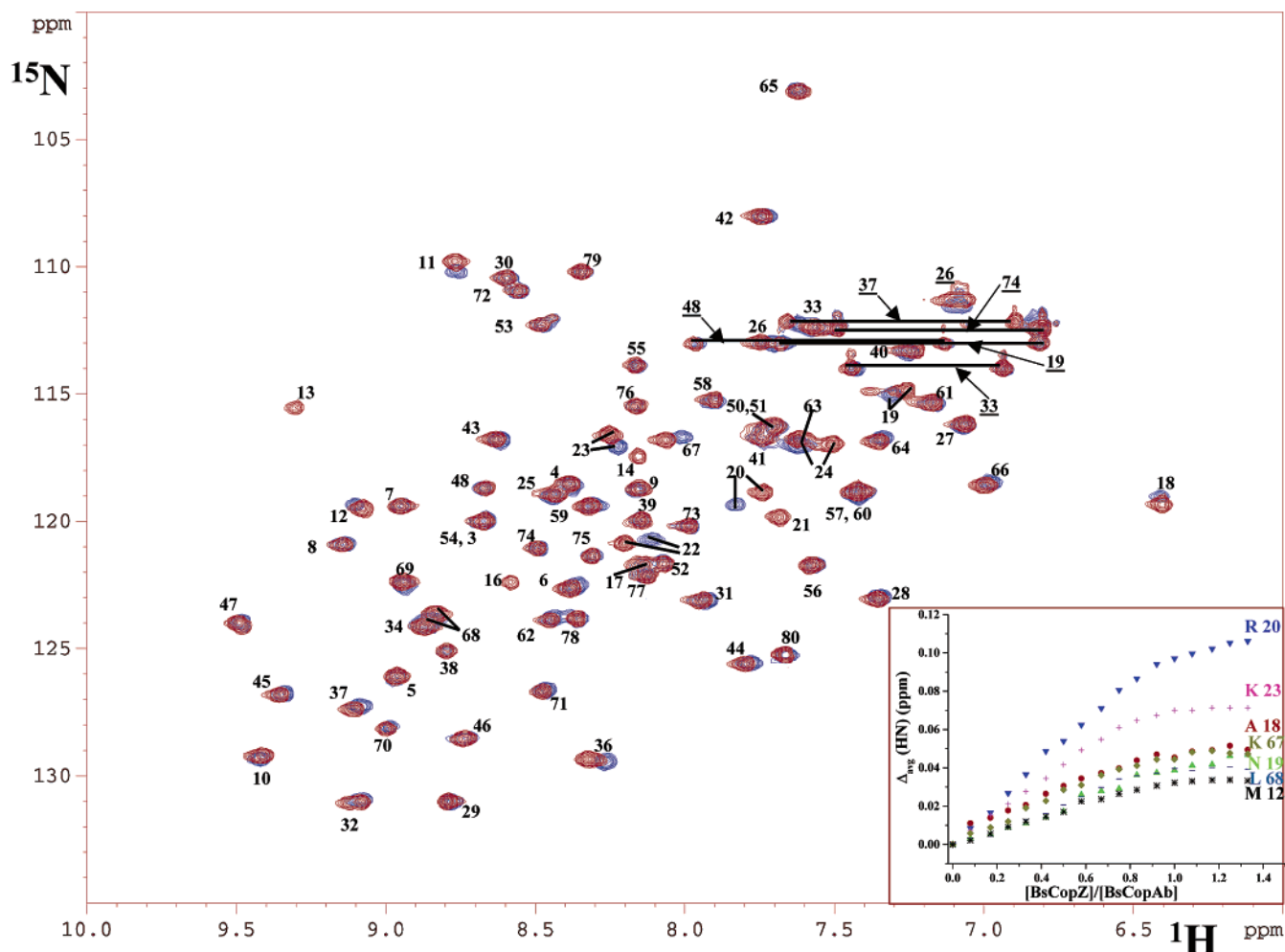
FIGURE 4: $^{15}N-^{1}H$ HSQC spectra (600 MHz, 298 K) of Cu(I)-^{15}N BsCopAb (red) and of the ^{15}N BsCopAb:BsCopZ (1:1) mixture (blue). The peaks due to side chain NHs are indicated with underlined numbers. The inset shows the weighted-average chemical shift differences $\Delta_{avg}(HN)$ (see text) for some BsCopAb residues around the metal site as a function of BsCopZ concentration.

bound protein was found to be 9.17 ± 0.79 ns from the R_2/R_1 ratios. This value is consistent with a large fraction of the protein being in a dimeric state (40).

The presence of R_{ex} contributions to transverse relaxation of backbone amide nitrogens was evaluated by measuring R_2 as a function of the τ_{CPMG} duration which produces different effective field strengths, ν_{eff}, as given by eq 3. A dependence of R_2 on ν_{eff} indicates the presence of exchange phenomena occurring in the range $500-100$ μs, as determined by our experimental conditions. The analysis was performed for Cu(I)-BsCopZ and Cu(I)-BsCopA. These results are summarized in Supporting Information together with the correlation time of the exchange process, τ_{ex}, obtained from fitting to eq 2.

In Cu(I)-^{15}N BsCopZ, 13 residues show a dependence of R_2 on ν_{eff}. The ^{15}N resonances of residues Cys 13 and Gln 14 belonging to loop 1 have a bad signal-to-noise ratio and therefore cannot be accurately integrated. Most of the residues belonging to the metal-binding region (loop 1 and first part of helix α1) and helix α2 show R_2 values significantly larger than the average value (Figure 5). This could be due to anisotropic tumbling of the protein, which could be related to its dimeric state, or to chemical exchange phenomena. The R_2/R_1 analysis does not distinguish between the effects of motional anisotropy and chemical exchange. It has been previously suggested that analysis of the product

R_2R_1 discriminates between the effects of chemical exchange and motional anisotropy (41). The product of R_2 and R_1 allows us to identify the presence of exchange processes only for residues 12, 15, 17, 46, and 54. Therefore, the increased R_2 values of the residues belonging to helix α2 (53-63) are predominantly due to rotational anisotropy of the dimer, while the residues of the metal-binding region experience conformational exchange processes. Indeed, a large number of residues experiencing a dependence of their R_2 rates on ν_{eff} are located in this region. In Cu(I)-BsCopAb, the number of residues displaying a dependence of R_2 on ν_{eff} is 9 (Supporting Information), which are located around the metal-binding loop. Residues involved in conformational exchange processes for the Cu(I)-bound forms of BsCopZ and BsCopAb are shown in Figure 6. The dynamic characterization of the two copper proteins identifies an overall larger mobility for the BsCopZ protein with respect to BsCopA. However, the metal-binding site residues of both proteins experience conformational exchange processes.

Dynamic Characterization of the Protein Complex. In the ^{15}N BsCopAb:^{15}N BsCopZ (1:1) mixture, R_2 and R_1 values can be determined for 60 ^{15}N nuclei of BsCopAb. The average values of R_2 and R_1 relaxation rates are 11.62 ± 1.71 s^{-1} and 1.60 ± 0.10 s^{-1}, respectively. In Figure 7a, R_2 and R_1 values of BsCopAb ^{15}NH cross-peaks in the complex are compared with those of the isolated apo-BsCopAb. The
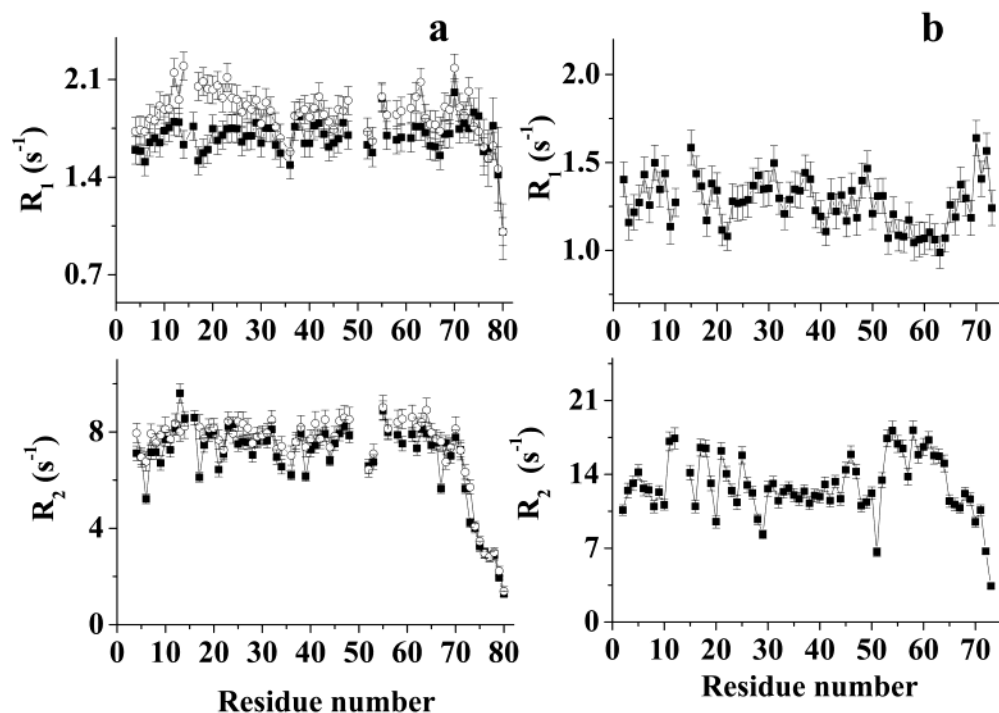
FIGURE 5: (a) ^{15}N relaxation parameters R_2 (bottom) and R_1 (top) of the backbone nitrogens of Cu(I)-BsCopAb (■) and of apo-BsCopAb (○). (b) ^{15}N relaxation parameters R_2 (bottom) and R_1 (top) of the backbone nitrogens of Cu(I)-BsCopZ.
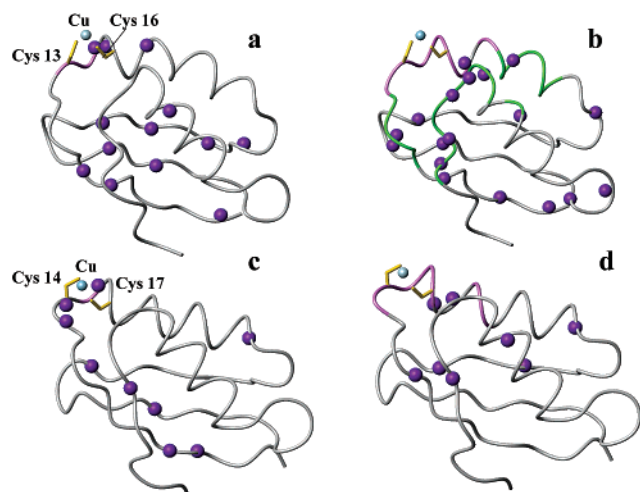

FIGURE 6: Mapping of ^{15}N mobility in the microsecond−millisecond time scale on the protein frame of Cu(I)-BsCopZ (a), BsCopZ in the 1:1 mixture (b), Cu(I)-BsCopAb (c), and BsCopAb in the 1:1 mixture (d). ^{15}N atoms of residues experiencing exchange processes are shown as violet spheres. The HN resonances of residues not detected or broadened are colored in pink, and those experiencing two conformations are colored in green. The metal ligands and the copper ions are also shown.

transverse relaxation rates show, overall, a relevant increase with respect to isolated apo-BsCopAb, while the R_1 values show a global decrease. However, R_2 and R_1 values of BsCopAb in the complex show a trend similar to that of the isolated apo form. In particular, the C-terminal region still experiences R_2 values lower than 1σ from the mean value. The τ_m value was found to be 8.2 ± 0.6 ns. This value is consistent with about 70% formation of the protein−protein complex. The same analysis was performed on the BsCopZ in the presence of unlabeled apo-CopAb, for 67 ^{15}N nuclei, and no relevant increases of the transverse relaxation rates were observed with respect to the pure Cu(I)-BsCopZ

(average values of R_1 and R_2 12.22 ± 1.29 s^{-1} and 1.34 ± 0.19 s^{-1}, respectively) (Figure 7b), providing a τ_m value of 9.10 ± 0.94 ns. This value is comparable to that found for the isolated protein, which is essentially dimeric, and it is consistent with the 1:1 stoichiometry of the complex.

R_2 measurements as a function of τ_{CPMG} length were performed on the 1:1 mixture to identify conformational exchange processes. The number of residues displaying a dependence of R_2 on the τ_{CPMG} length increases to 18 for BsCopZ, while no significant differences are observed for BsCopAb, with the exception of the first turn of helix $\alpha1$, which displays conformational exchange processes only in the complex (Figure 6 and Supporting Information). The dynamic characterization of the BsCopZ protein in the complex points to a different mobility around the copper binding region with respect to the free state; indeed, the occurrence of conformational exchange processes is observed in loop 5 and loop 3 when the complex with BsCopAb is formed. Moreover, most of the residues in these regions experience the presence of two forms in slow exchange on the NMR time scale (see before), proving an overall increase of the dynamic properties of the complexed BsCopZ.

DISCUSSION

The CopZ−CopA Complex. Titrations of Cu(I)-BsCopZ with apo-BsCopAb, apo-BsCopAb with Cu(I)-BsCopZ, and Cu(I)-BsCopAb with apo-BsCopZ indicated that the two proteins interact one with the other, forming a complex with a 1:1 stoichiometry and an affinity of about 10^4 M^{-1}. The overall reorientational correlation time is consistent with the formation of ∼70% of the complex in the 1:1 protein ratio at millimolar concentrations. For all BsCopAb residues and most of the BsCopZ residues, a single signal is detected in the 1:1 complex, which indicates an essentially fast exchange regime between the free and the complex states. Some signals show just chemical changes, while others, experiencing larger
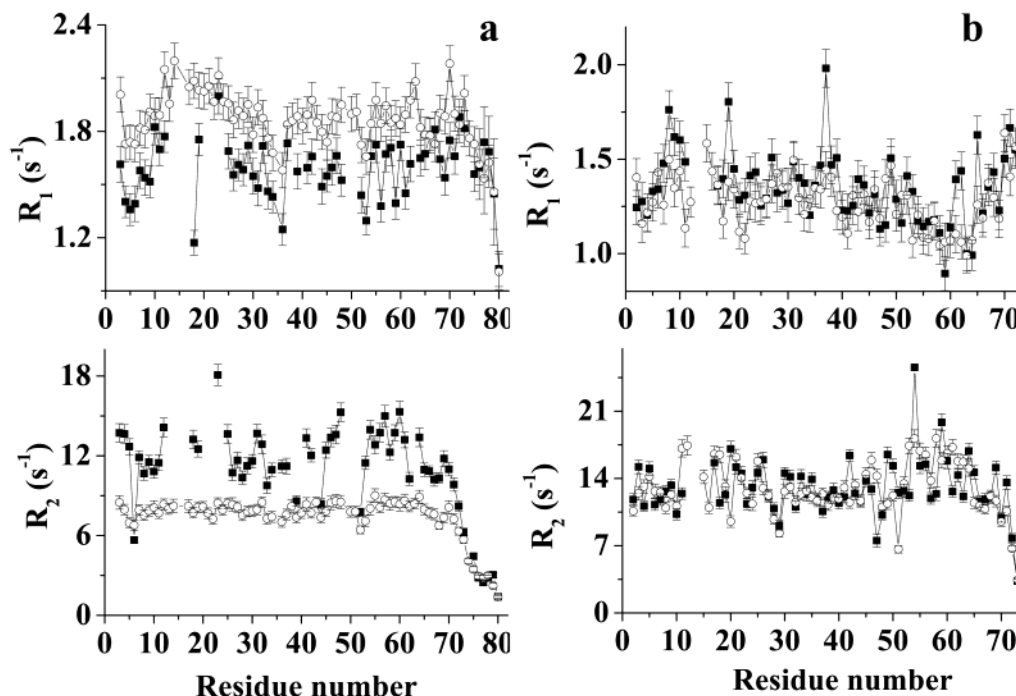
FIGURE 7: (a) ^{15}N relaxation parameters R_2 (bottom) and R_1 (top) of the backbone nitrogens of apo-BsCopAb (○) and of BsCopAb in the presence of BsCopZ (■) at a 1:1 ratio. (b) ^{15}N relaxation parameters R_2 (bottom) and R_1 (top) of the backbone nitrogens of Cu(I)-BsCopZ (○) and of BsCopZ in the presence of BsCopAb (■) at a 1:1 ratio.

chemical shift variations, show also some broadening, presumably due to the exchange between the free proteins and the complex not faster than the chemical shift difference between the corresponding signals.

The largest chemical shift difference between a signal in the isolated proteins and a signal in the complex, without significant line broadening, is ∼90 Hz (for the ^1HN proton of the backbone amide of Ala 18 of BsCopAb), which yields a lower limit of ∼600 s^{-1} for the rate constant of the complex dissociation, k_D. This value is half of that found for the Atx1/Ccc2a complex (13).

The changes in chemical shift values are located, for both proteins, in the metal-binding region and other protein regions surrounding it, particularly loop 5. The chemical shift changes are mapped on the protein frames for both partners and shown in Figure 8, which also reports the electrostatic surface of the two proteins. As already suggested by us (22, 23), the driving force for the molecular recognition of the two proteins is determined by the electrostatic complementarity of the two interacting proteins. This electrostatic potential guidance for the protein attraction was also found for Atx1 and Ccc2a (13) and for the interaction between CopZ and CopY from *E. hirae* (19). In the Atx1−Ccc2a complex, the residues experiencing spectral changes upon complex formation were located in the same regions, i.e., the metal-binding site, loop 5, and helix α1. However, Atx1 has an extensive positive surface whereas its analogue, BsCopZ, possesses a negative surface. Consistently with this inversion of charge, Ccc2a has a negative surface near the copper binding region, which contains positively charged residues in BsCopAb.

The size of the chemical shift changes are smaller than those observed in the Atx−Ccc2a complex (13). As the affinity of the latter two proteins is similar (about 70% of the complex formed in a 1:1 mixture) to that of the present

system, we may argue that the structural changes induced by protein−protein interactions are smaller in the present case. The possibility of multisite interactions, which would average the spectral changes, can be ruled out on the basis that the changes are located, for both proteins, in the same areas and involve the same residues in both titrations. The complex and the single proteins are exchanging fast to each other on the NMR time scale. The same average species is obtained when mixing the two proteins, regardless of which is the protein carrying the copper ion.

If the spectrum of the complex is compared with those of the apo and copper-bound forms of the proteins, it may be concluded that BsCopZ in the complex is largely present as the apo form and BsCopAb is largely in the copper-bound form. Indeed, large spectral changes of the residues nearby the metal-binding ligands are observed for apo-BsCopAb upon complex formation, whereas minor changes occur when Cu(I)-BsCopAb is titrated with apo-BsCopZ. Looking at the BsCopZ side, when the copper-loaded form is titrated with apo-BsCopAb, residues in the 8−16, 22−25, and 62−67 regions initially broaden and then have features similar to those in the apo form: some signals change the chemical shift values, some of them show a second signal due to the minor form present in the apo-BsCopZ, and signals 12−16 disappear.

A coordination number of three around copper(I) can be an intermediate in the complex that would allow BsCopZ and BsCopAb to exchange from the complex as apo forms. This "three-coordinative" mechanism is also supported by NMR studies performed on Cu(I) and Hg(II) glutathione complexes (42, 43). Indeed, those studies showed that the metal is rapidly exchanged among thiol ligands via formation of a transient Hg(II)−(thiol)$_3$ complex and that the high thermodynamic stability of Cu(I)−S bonds in the complexes is coupled with their kinetic lability. The different overall
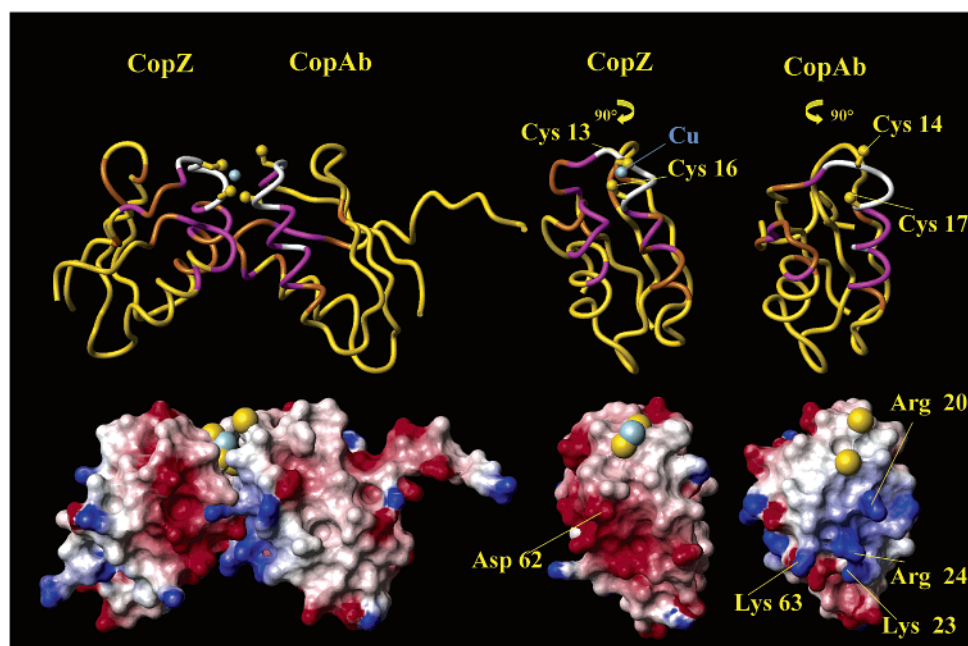
FIGURE 8: Structural model of the BsCopAb−BsCopZ complex model determined on the basis of the mapping of the chemical shift changes. Color code: magenta, $\Delta_{avg}(HN) > 0.03$ ppm; orange, $0.03 < \Delta_{avg}(HN) < 0.015$ ppm; yellow, $\Delta_{avg}(HN) < 0.015$ ppm; white, not observed. An electrostatic surface representation of the Cu(I) form of BsCopZ and apo-BsCopAb is shown in the lower panels. The positively charged, negatively charged, and neutral amino acids are represented in blue, red, and white, respectively. The views on the right side are the molecules rotated by 90° to allow interaction surfaces to be seen, which are facing the reader.

charge between the two proteins favors protein−protein interactions, and the metal ion favors a facile exchange via a series of three-coordinate intermediates (*44*).

A structural model of the complex was obtained starting from the X-ray structure of the dimeric state of the human homologue Atx1 (Hah1) (*45*). Then, the relative orientation of the two molecules was optimized by placing at the complex interface the residue experiencing chemical shift perturbation and by maximizing the interaction surface and contacts between oppositely charged residues (Figure 8). Among the latter it is worth noting the interaction, Asp 62 BsCopZ /Lys 23 BsCopAb, which involves residues conserved in homologous bacterial sequences and that between the conserved Arg 20 BsCopAb/Glu 21 BsCopZ, whose chemical shift values are strongly affected by addition of the partner.

The dynamics data showed that isolated Cu(I)-BsCopZ forms a homodimer, whereas isolated BsCopAb is in a monomeric state. When these two proteins are in a 1:1 mixture, their reorientational correlation time τ_m is consistent with a sizable percentage of proteins in the dimeric state. Therefore, one BsCopZ protein of the homodimer should exchange with the protein partner BsCopAb, thus forming a heterodimeric species, which allows for the facile transfer of copper between partner proteins. As we discussed above, there is an electrostatic complementary attraction between BsCopZ and BsCopAb, which should stabilize the heterodimeric complex with respect to the homodimeric BsCopZ species. Similar models of copper transfer complexes which involve a heterodimeric or heterotetrameric intermediate have been proposed for the interaction between the dimeric or monomeric yeast SOD and its copper chaperone, CCS (*46*−*48*). Therefore, this kind of mechanism involving equilibrium between homo- and heterodimeric species can be a general

means that organisms use to transfer copper ions and keep their level under control in the cytoplasm.

Copper Trafficking in B. subtilis in Comparison with Other Bacterial Systems. In *B. subtilis*, a Gram-positive bacterium, the gene located upstream of the *CopZ* encodes a protein of unknown function, whose secondary structure prediction is a full α-helical fold, while the *CopA* neighbor gene encodes another CPx-type ATPase whose sequence is significantly homologous to other zinc and cadmium transporters (*49*, *50*). Indeed, the metal-binding consensus motif of the N-terminal region contains a negatively charged Asp residue which is conserved among a class of CPx-type ATPases defined as ZntA homologues (*21*) and which may facilitate the binding of a divalent cation. Moreover, residues surrounding the CPx motif in the transmembrane region, which is involved with the metal transport, are characteristic of the zinc and cadmium ATPases (*51*).

In *E. hirae*, another Gram-positive bacterium, the Cop operon consists of four genes that encode a metalloregulated repressor (CopY), a copper chaperone (CopZ), and two CPx-type copper ATPases (CopA and CopB) (*18*). The gene organization of this operon is similar to that found in *B. subtilis* but with some significant differences. Previous studies indicated that CopA in *E. hirae* is responsible for copper uptake under copper limiting conditions and CopB for copper export if copper reaches toxic levels (*16*). It has been recently also shown that CopZ interacts both with its repressor CopY and with CopA (*19*, *20*), thus suggesting that CopZ routes copper to different intracellular targets, including CopY, which regulates the transcription of the Cop operon (*52*).

In the Cop operons of these two Gram-positive bacteria, the gene encoding CopB in the *E. hirae* corresponds, in *B. subtilis*, to a gene encoding a probable zinc/cadmium

ATPase. From sequence homology search, no CopB gene homologue can be identified in the genome of *B. subtilis*, indicating that the *B. subtilis* operon does not contain a CopB homologue. This result leads us to suggest that the copper trafficking in *B. subtilis* is differently organized with respect to *E. hirae*. This hypothesis is also consistent with the large variety of the Cop operon organization found in bacterial organisms (*14*, *53*). For example, the genome of the Gram-negative *E. coli* bacterium appears to encode a Cu-trans-locating efflux pump ATPase but not a Cu chaperone, and it has been proposed that the a Cu chaperone is obtained by specific proteolytic separation of the N-terminal domain of the ATPase (*54*). Another interesting case is observed for the genome of *Archaeoglobus fulgidus*, which contains CopA and CopB proteins and a putative copper chaperone (*55*), whose genes appear similar to those of CopA and CopB from *E. hirae* (percentage identity, 41% and 40%, respectively). It has been proposed that CopA transports Cu(I) out of the cell (*55*), at variance with CopA from *E. hirae*. In this regard, *A. fulgidus* CopA appears similar to its *E. coli* orthologue (*56*). The diversity of the Cop operon organization in *B. subtilis* with respect to that one in *E. hirae* may reflect a different role for CopA ATPase which can drive, depending on the organisms, the influx or the efflux of copper to or from CopZ.

CONCLUDING REMARKS

In the present investigation the complex between CopZ and CopAb from *B. subtilis* through ^{15}N$-^{1}$H HSQC spectroscopy and ^{15}N mobility studies has been characterized. The first set of experiments provides evidence of the interaction, and through ^{15}N chemical shift differences a model of the complex can be proposed. The mobility studies complete the picture by providing also the dynamic properties of the complex. It is found that copper in the complex is largely transferred from CopZ to CopA. This suggests an involvement of the proteins in the copper detoxification process. Some variability in the role of CopA protein in the copper transport and of the entire process has been analyzed within the genomes of some bacterial organisms. The progress in the knowledge of the copper trafficking mechanisms in various organisms indicates an intriguing differentiation of the roles of homologue proteins.

SUPPORTING INFORMATION AVAILABLE

One figure with ^{1}H and ^{15}N amide chemical shift differences between the pure Cu(I)-^{15}N BsCopAb and the ^{15}N BsCopAb:BsCopZ (1:1) mixture and two tables comprising residues whose NH group is involved in conformational exchange processes in BsCopZ and BsCopAb proteins. This material is available free of charge via the Internet at http://pubs.acs.org.

REFERENCES

1. Puig, S., and Thiele, D. J. (2002) *Curr. Opin. Chem. Biol. 6*, 171−180.
2. Huffman, D. L., and O'Halloran, T. V. (2001) *Annu. Rev. Biochem. 70*, 677−701.
3. Harrison, M. D., Jones, C. E., Solioz, M., and Dameron, C. T. (2000) *Trends Biochem. Sci. 25*, 29−32.
4. Dancis, A., Yuan, D. S., Haile, D., Askwith, C., Elde, D., Moehle, C., Kaplan, J., and Klausner, R. D. (1994) *Cell 76*, 393−402.
5. Dancis, A., Haile, D., Yuan, D. S., and Klausner, R. D. (1994) *J. Biol. Chem. 269*, 25660−25667.
6. Pena, M. M. O., Lee, J., and Thiele, D. J. (1999) *J. Nutr. 129*, 1251−1260.
7. Zhou, B., and Gitschier, J. (1997) *Proc. Natl. Acad. Sci. U.S.A. 94*, 7481−7486.
8. Askwith, C., Eide, D., Van Ho, A., Bernard, P. S., Li, L., Davis-Kaplan, S., Sipe, D. M., and Kaplan, J. (1994) *Cell 76*, 403−410.
9. Rae, T., Schmidt, P. J., Pufahl, R. A., Culotta, V. C., and O'Halloran, T. V. (1999) *Science 284*, 805−808.
10. Fu, D., Beeler, T. J., and Dunn, T. M. (1995) *Yeast 11*, 283−292.
11. Arnesano, F., Banci, L., Bertini, I., Huffman, D. L., and O'Halloran, T. V. (2001) *Biochemistry 40*, 1528−1539.
12. Banci, L., Bertini, I., Ciofi-Baffoni, S., Huffman, D. L., and O'Halloran, T. V. (2001) *J. Biol. Chem. 276*, 8415−8426.
13. Arnesano, F., Banci, L., Bertini, I., Cantini, F., Ciofi-Baffoni, S., Huffman, D. L., and O'Halloran, T. V. (2001) *J. Biol. Chem. 276*, 41365−41376.
14. Jordan, K., Natale, D. A., and Galperin, M. Y. (2002) *Trends Biochem. Sci. 25*, 480−481.
15. Rensing, C., Ghosh, M., and Rosen, B. P. (1999) *J. Bacteriol. 181*, 5891−5897.
16. Odermatt, A., Suter, H., Krapf, R., and Solioz, M. (1993) *J. Biol. Chem. 268*, 12775−12779.
17. Solioz, M., and Odermatt, A. (1995) *J. Biol. Chem. 270*, 9217−9221.
18. Odermatt, A., Suter, H., Krapf, R., and Solioz, M. (1992) *Ann. N.Y. Acad. Sci. 671*, 484−486.
19. Cobine, P. A., George, G. N., Jones, C. E., Wickramasinghe, W. A., Solioz, M., and Dameron, C. T. (2002) *Biochemistry 41*, 5822−5829.
20. Multhaup, G., Strausak, D., Bissig, K. D., and Solioz, M. (2001) *Biochem. Biophys. Res. Commun. 288*, 172−177.
21. Arnesano, F., Banci, L., Bertini, I., Ciofi-Baffoni, S., Molteni, E., Huffman, D. L., and O'Halloran, T. V. (2002) *Genome Res. 12*, 255−271.
22. Banci, L., Bertini, I., Ciofi-Baffoni, S., D'Onofrio, M., Gonnelli, L., Marhuenda-Egea, F. C., and Ruiz-Dueñas, F. J. (2002) *J. Mol. Biol. 317*, 415−429.
23. Banci, L., Bertini, I., Del Conte, R., Markey, J., and Ruiz-Dueñas, F. J. (2001) *Biochemistry 40*, 15660−15668.
24. Hubbard, T. J. P., Murzin, A. G., Brenner, S. E., and Chothia, C. (1997) *Nucleic Acids Res. 25*, 236−239.
25. Huffman, D. L., and O'Halloran, T. V. (2000) *J. Biol. Chem. 275*, 18611−18614.
26. Kay, L. E., Nicholson, L. K., Delaglio, F., Bax, A., and Torchia, D. A. (1992) *J. Magn. Reson. 97*, 359−375.
27. Orekhov, V. Y., Pervushin, K. V., and Arseniev, A. S. (1994) *Eur. J. Biochem. 219*, 887−896.
28. Peng, J. W., and Wagner, G. (1994) *Methods Enzymol. 239*, 563−596.
29. Marion, D., and Wüthrich, K. (1983) *Biochem. Biophys. Res. Commun. 113*, 967−974.
30. Piotto, M., Saudek, V., and Sklenar, V. (1992) *J. Biomol. NMR 2*, 661−666.
31. Grzesiek, S., and Bax, A. (1993) *J. Am. Chem. Soc. 115*, 12593−12594.
32. Eccles, C., Güntert, P., Billeter, M., and Wüthrich, K. (1991) *J. Biomol. NMR 1*, 111−130.
33. Palmer, A. G., III, Rance, M., and Wright, P. E. (1991) *J. Am. Chem. Soc. 113*, 4371−4380.
34. Peng, J. W., and Wagner, G. (1992) *Biochemistry 31*, 8571−8586.
35. Zinn-Justin, S., Berthault, P., Guenneugues, M., and Desvaux, H. (1997) *J. Biomol. NMR 10*, 363−372.
36. Mandel, M. A., Akke, M., and Palmer, A. G., III (1995) *J. Mol. Biol. 246*, 144−163.
37. Tjandra, N., Feller, S. E., Pastor, R. W., and Bax, A. (1995) *J. Am. Chem. Soc. 117*, 12562−12566.
38. Bloom, M., Reeves, L. W., and Wells, E. J. (1965) *J. Chem. Phys. 42*, 1615−1624.
39. Garrett, D. S., Seok, Y. J., Liao, D. I., Peterkofsky, A., Gronenborn, A. M., and Clore, G. M. (1997) *Biochemistry 36*, 2517−2530.
40. Banci, L., Bertini, I., Del Conte, R., Mangani, S., and Meyer-Klaucke, W. (2003) *Biochemistry* (in press).
41. Kneller, J. M., Lu, M., and Bracken, C. (2002) *J. Am. Chem. Soc. 124*, 1852−1853.
42. Corazza, A., Harvey, I., and Sadler, P. J. (1996) *Eur. J. Biochem. 236*, 697−705.

43. Cheesman, B. V., Arnold, A. P., and Rubenstein, D. L. (1988) *J. Am. Chem. Soc. 110*, 6359−6364.

44. Pufahl, R. A., Singer, C. P., Peariso, K. L., Lin, S.-J., Schmidt, P. J., Fahrni, C. J., Cizewski Culotta, V., Penner-Hahn, J. E., and O'Halloran, T. V. (1997) *Science 278*, 853−856.

45. Wernimont, A. K., Huffman, D. L., Lamb, A. L., O'Halloran, T. V., and Rosenzweig, A. C. (2000) *Nat. Struct. Biol. 7*, 766−771.

46. Torres, A. S., Petri, V., Rae, T. D., and O'Halloran, T. V. (2001) *J. Biol. Chem.* 38410−38426.

47. Hall, L. T., Sanchez, R. J., Holloway, S. P., Zhu, H., Stine, J. E., Lyons, T. J., Demeler, B., Schirf, V., Hansen, J. C., Nersissian, A. M., Valentine, J. S., and Hart, P. J. (2000) *Biochemistry 39*, 3611−3623.

48. Lamb, A. L., Torres, A. S., O'Halloran, T. V., and Rosenzweig, A. C. (2001) *Nat. Struct. Biol. 8*, 751−755.

49. Christakos, N., Babrielides, C., and Rhoten, W. (1989) *Endocr. Rev. 10*, 3−26.

50. Rensing, C., Mitra, B., and Rosen, B. P. (1998) *Biochem. Cell Biol. 76*, 787−790.

51. Tottey, S., Rich, P. R., Rondet, S. A. M., and Robinson, N. J. (2001) *J. Biol. Chem 276*, 19999−20004.

52. Odermatt, A., and Solioz, M. (1995) *J. Biol. Chem. 270*, 4349−4354.

53. Jordan, K., Natale, D. A., Koonin, E. V., and Galperin, M. Y. (2001) *J. Mol. Evol. 53*, 622−633.

54. Wasinger, V. C., and Humphery-Smith, I. (1998) *FEMS Microbiol. Lett. 169*, 375−382.

55. Mandal, A. K., Cheung, W. D., and Argüello, J. M. (2002) *J. Biol. Chem. 277*, 7201−7208.

56. Rensing, C., Fan, B., Sharma, R., Mitra, B., and Rosen, B. P. (2000) *Proc. Natl. Acad. Sci. U.S.A. 97*, 652−656.

57. Bodenhausen, G., and Ruben, D. J. (1980) *Chem. Phys. Lett. 69*, 185−188.

58. Wider, G., Macura, S., Kumar, A., Ernst, R. R., and Wüthrich, K. (1984) *J. Magn. Reson. 56*, 207−234.

59. Wider, G., Neri, D., Otting, G., and Wüthrich, K. (1989) *J. Magn. Reson. 85*, 426−431.

60. Griesinger, C., Otting, G., Wüthrich, K., and Ernst, R. R. (1988) *J. Am. Chem. Soc. 110*, 7870−7872.